

# Design, Control, and Energetics of an Electrically Actuated Legged Robot

Pedro Gregorio, Mojtaba Ahmadi, and Martin Buehler, *Member, IEEE*

**Abstract**—To study the design, control and energetics of autonomous dynamically stable legged machines we have built a planar one-legged robot, the ARL Monopod. Its top running speed of 4.3 km/h (1.2 m/s) makes it the fastest electrically actuated legged robot to date. We adapted Raibert's control laws for the low power electric actuation necessary for autonomous locomotion and performed a detailed energetic analysis of our experiments. A comparison shows that the ARL Monopod with its 125 W average power consumption is more energy efficient than previously built robots.

## I. INTRODUCTION

**L**EGGED robots capable of dynamic operation and active balance have the potential for similar mobility, efficiency, and dexterity as their biological counterparts. Such robots would be able to operate in a much larger range of environments and surface conditions than current wheeled and tracked vehicles. Moreover, similar system design and control advances would benefit applications beyond those requiring traditional locomotion, for example dextrous mechanisms for the inspection of power lines, steel trusses, or pipe systems. Once stable and autonomous legged systems are feasible and affordable, there will be no lack of applications. While the Ambulatory Robotics Lab (ARL) Monopod is not yet power-autonomous, its low power and unprecedented efficiency represent important milestones toward that goal.

Legged robots generally fall into one of two classes; those capable of dynamic operation and those designed for static walking. In static walkers, stability is assured through kinematics by keeping the center of mass of the machine above the polygon formed by the supporting feet [1]. As a consequence, these machines have at least four legs (or very large feet) although they are often built with six legs to improve mobility. Static walkers do not balance actively and since dynamics of motion are not considered, speeds are low. Dynamic robots which balance actively require fewer legs and have a greater potential for speed and power efficiency.

Even though legged robots were proposed a long time ago [2], experimental research on actively balanced legged robots began with Matsuoka's planar one-legged hopping machine [3] which was sliding on an inclined plane and was thrust

by an electric solenoid. The first walking machine with active balance was built by Miura and Shimoyama [4]. It operated with stiff legs, similar to humans on stilts. Our work has been inspired primarily by Raibert [5] who has led the field of dynamically stable legged locomotion during the past 15 years. He built and controlled successfully one-, two-, and four-legged robots. Except for the first one-legged planar hopper, which was pneumatically actuated, his designs use powerful hydraulic actuators and rely on pneumatics for the leg spring only. By effectively eliminating power constraints, he was able to focus on robot design and control issues. This strategy was eminently successful—most of the robots were based on an almost standardized set of parts and controlled by some derivative of the tri-partitioned decoupled control developed for the original one-legged planar hopper. The first application of Raibert's design and control ideas to an electrically actuated robot comes from Papantoniou [6] whose one-legged robot performs the "compliant walk" gait to cope with power limitations. Today, there are many research labs devoted to dynamic locomotion. A broader review of research in legged locomotion can be found in [5].

This paper is organized as follows. In Section II we describe the mechanical design of the ARL Monopod. The two transmission mechanisms (one for the robot's hip and one for the leg) are optimized for electric actuation and are the key to the successful and energy efficient operation of the robot. In Section III, we describe the adaptation of Raibert's controller for our robot and demonstrate its performance with experimental runs. A detailed energetic analysis of our robot's running as well as an efficiency comparison with other land vehicles and other modes of locomotion is provided in Sections IV and V. These results can be used as a basis for further energy improvements. The paper concludes with a discussion of our results and a proposal for future work.

## II. EXPERIMENTAL HARDWARE

The success of the ARL Monopod is based on a systems approach, where the mechanical and the controller design are closely coupled and based on our knowledge of the operating regime. In this section we describe the overall mechanical design, and detail the hip transmission design as an example of this systems approach.

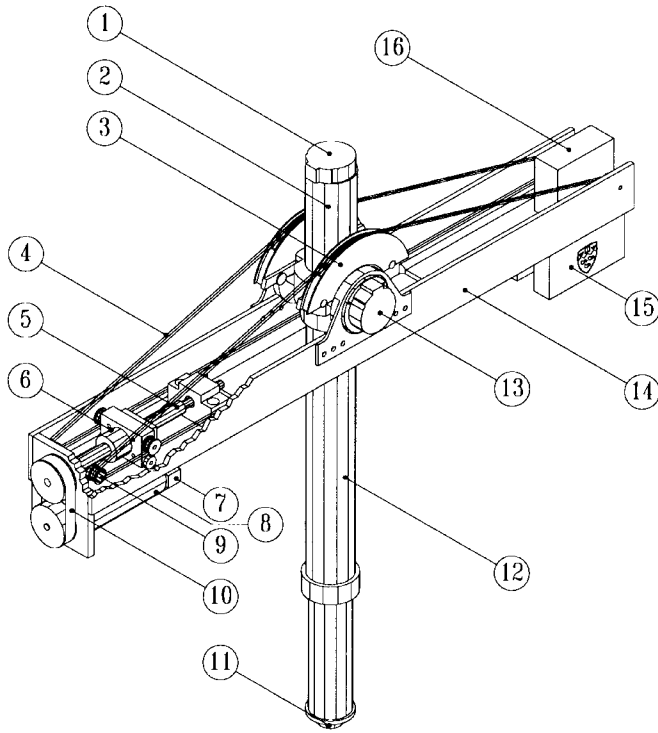
### A. ARL Monopod

While the actuation and transmission systems of the ARL Monopod are quite different from Raibert's one-legged robot

Manuscript received August 12, 1995; revised March 20, 1996. This work was supported by the Natural Sciences and Engineering Research Council of Canada under Grant OGPO-138117 and a Junior Industrial Research Chair, held by M. Buehler.

P. Gregorio is with Solutions By Design, Montreal, P.Q., Canada H2R 2S4. M. Ahmadi and M. Buehler are with the Center for Intelligent Machines, McGill University, Montreal, P.Q., Canada H3A 2A7.

Publisher Item Identifier S 1083-4419(97)03880-6.



1 leg motor sensor	7 hip motor sensor	13 hip sensor
2 leg motor	8 hip motor	14 body
3 hip pulley	9 cable idler	15 servo amplifiers
4 cables	10 timing belt	16 counter weight
5 ball screw	11 rubber toe	
6 ball nut	12 leg	

Fig. 1. ARL Monopod assembly drawing.

design [5] the overall size and kinematics are similar: The robot consists of a prismatic leg, which is attached to the body via a revolute hip joint, as shown in Fig. 1.

The leg is a linear arrangement of an electric motor, a ballscrew, a spring, and the lower leg. Its purpose is to support a quasipassive vertical oscillation between the body mass and the leg spring via periodic excitation by the leg motor. In contrast to Raibert's design, we have replaced the hydraulic actuator–pneumatic spring combination with an electric motor–ballscrew–coilspring system. In the process, there are many design parameters that have to be selected properly to be able to transfer sufficient energy into the system during the short stance phase. This process is similar the hip design described below, and can be found in [7].

The leg connects to the body via a revolute hip joint, which is actuated by a pulley–cable–ball screw–electric motor system. The cables (4) are fixed at one end to the hip pulley (3) which actuates the leg (12). At the other end, the cables run over idlers (9) and attach to the ball nut of a high efficiency ball screw (6), (5). The ball screw is actuated by the hip motor (8) through a timing belt (10) and pulleys and converts motor torque into an axial force at the ball nut. This ball nut force, in turn, tensions the cables which actuates the hip pulley.

This overall design satisfies several goals. The body inertia should be high compared to that of the leg in order to minimize the pitching motion of the body in response to leg swinging.

At the same time, body mass should be kept low to minimize energy consumption for vertical motion. Both requirements are satisfied by a long body whose mass is concentrated at the ends. To generate the 55 Nm hip torque required for forward running from our 1.8 Nm stall torque, 80 W motors, the transmission system provides a 30:1 gear ratio.

The motion of the robot is constrained to a vertical plane via a low friction “planarizer”—a three degree of freedom prismatic–prismatic–revolute mechanism mounted above a treadmill. This setup facilitates systematic experimentation, while preserving all the complexity of control and energetics in the plane. The control algorithms discussed below together with I/O, signal processing, data logging, safety, etc., executed on a transputer-based real-time control board [8] which issues motor torque commands at a rate of 1 kHz.

### B. Hip Transmission Design

This section describes our optimization procedure for selecting the parameters of the hip actuation system for two different operating conditions. The first is direct actuation, which is the topic of this paper, and second compliant actuation, where a spring is inserted in the transmission cable for our ongoing research on passive dynamic running [9]. We have assumed as a given the electric motor characteristics, and search for the hip pulley radius  $R$ , the ball screw lead  $r_s$ , and the hip compliance stiffness  $k_h$ . For direct actuation,  $k_h$  is set to a large value equal to the cable stiffness. The design requires that the motor's torque–speed curve not be exceeded while the leg swings during running.

We simulated the hip transmission dynamics and forced the hip actuator to track a sinusoidal trajectory similar to the expected trajectory for robot running. Results from vertical hopping experiments [7] were used to select the parameters of this sinusoidal trajectory. A frequency of 2 Hz equal to the vertical hopping frequency and an amplitude of  $20^\circ$  corresponding to a running speed of 0.9 m/s were selected. The effects of body pitching were neglected.

The variables involved in the dynamical equations of the hip actuation system are given in Table I. Based on the equations of motion of a ball screw

$$\tau_m = r_s F_h + \alpha_h \ddot{p}_n$$

where

$$\alpha_h = J_s / r_s + r_s m_n$$

accounts for the combined inertia of the ball screw and ball nut, we obtain the tension in the hip cable

$$F_h = 2k_h(R\theta - p_n) + 2c_h(R\dot{\theta} - \dot{p}_n).$$

Approximating  $\sin(\theta) \approx \theta$  for small angles, the dynamics of the actuated hip are represented as

$$J_l \ddot{\theta} = R F_h - C_h \dot{\theta} - m_l g l_c \theta. \quad (1)$$

Solving (1) where the leg angle  $\theta$  follows the sinusoidal path  $\theta = \theta_0 \sin(\omega t)$  gives the motor torque

$$\tau_m = A \sin(\omega t) + B \cos(\omega t)$$

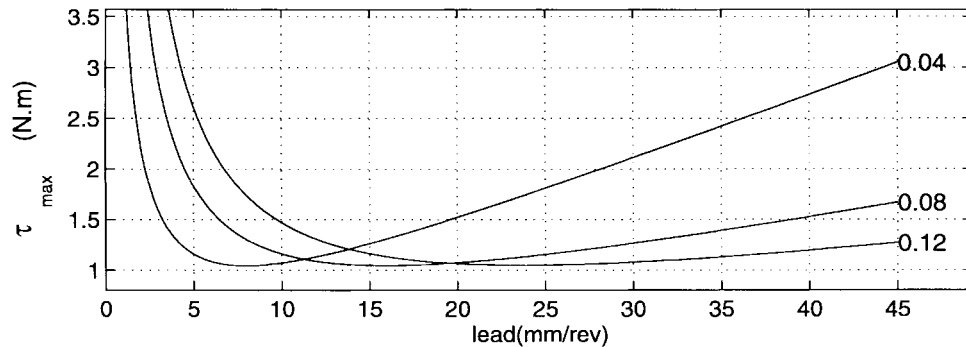


Fig. 2. Hip transmission design. Variations of maximum torque ( $\tau_{\max}$ ) versus lead ( $L$ ) for different values of pulley radius ( $R$ ).

TABLE I  
TRANSMISSION VARIABLES

$R$	hip pulley radius	$0.08(m)$
$\theta$	hip joint angle	$(rad)$
$C_h$	hip joint damping	$0.58(N/m/s)$
$F_h$	hip cable tension	$(N)$
$\tau_m$	hip motor torque	$(Nm)$
$\theta_s$	ball screw angle	$(rad)$
$r_s$	ball screw lead	$2.5E-3(m/rad)$
$J_s$	motor-screw inertia	$3.0E-4(kgm^2)$
$p_n$	ball nut position	$(m)$
$m_n$	ball nut mass	$0.25(kg)$
$F_n$	ball nut force	$(N)$
$\tau_n$	ball nut torque	$(Nm)$
$k_h$	hip compliance stiffness	$3600(N/m)$
$c_h$	hip compliance damping	$20(N/m/s)$
$m_l$	leg mass	$4.9(kg)$
$J_l$	leg inertia	$0.3(kgm^2)$
$l_c$	leg CG to hip joint distance	$0.015(m)$
$g$	gravitational acceleration	$9.81(m/s^2)$

where  $A$  and  $B$  are functions of the system design parameters, primarily the lever arm  $R$ , the stiffness  $k_h$  and ball screw lead  $r_s$ , as well as the parameters of the leg trajectory. We can now evaluate the motor's torque requirements as a function of leg speed,  $\tau_m(\omega)$ . The peak motor torque,  $\tau_{\max}$ , depends on the design parameters in a simple fashion

$$\tau_{\max} = \sqrt{A^2 + B^2}.$$

This maximum torque is shown in Fig. 2 for the direct actuation case with a leg swing amplitude of  $20^\circ$  and frequency of 2 Hz. The maximum hip motor torque,  $\tau_{\max}$  is plotted against the ball screw lead,  $L$ , expressed in mm/rev for three values of pulley radius  $R = 0.04$  m,  $R = 0.08$  m, and  $R = 0.12$  m.

The next step in the design process is to select the optimal combination of ball screw lead and pulley radius. Unfortunately, Fig. 2 is only one of many constraints. In addition, the motor characteristics impose a velocity dependent peak torque. Furthermore, ball screws are available only in coarsely discrete leads and lengths and their inertial parameters are only available via lookup tables. The cable tension  $F_h$  should be kept small because it affects the overall size and weight of our structures. Since we plan to use elastomeric springs in series

with the actuator in the future, the spring stiffness is limited to 5 kN/m due to energy storage limitations. The ball screw travel should be less than 0.1 m to limit the ball screw inertia and mass as well as body length. The design is further complicated by the necessity to meet the constraints for both direct and compliant actuation. The compliant case is facilitated by large pulley radius  $R$ , resulting in smaller torque requirements, but this increasing  $R$ , when combined with the optimum lead, increases motor velocity, acceleration, ball screw travel, and ball screw lead in the direct actuation case.

The final design parameters of lead  $L = 0.16$  mm/rev, pulley radius  $R = 0.08$  m, and spring constant  $k_h = 3600$  N/m satisfy all the constraints concerning pulley radius, ball screw lead, and maximum motor torque and velocity. In addition, this set of parameters minimizes the motor torque-speed requirements for compliant running by matching the natural frequency of the system with the frequency of the vertical oscillations of 2 Hz [7].

### III. CONTROL

The ARL Monopod, like any legged robot, is an intermittent dynamical system, whose equations of motion as well as state space dimensionality change between stance and flight phases. During flight, the system possesses five degrees of freedom and during stance only four. At all times, only two of these degrees of freedom are actuated, namely the hip angle and the leg actuator length.

Raibert developed a control strategy which decouples the complex coordinated running motion into three separate tasks; *hopping height control*, *forward speed control*, and *attitude control* [5]. Dynamic coupling effects (which increase with increasing velocity) between the different controllers are treated as perturbations. Hopping height is controlled during stance (see Fig. 3) by thrusting the leg actuator while body attitude is controlled simultaneously by applying hip torques. During flight, the hip actuator controls forward speed by placing the foot in proper location for the next touchdown, while the leg actuator simply retracts to its nominal position. To control our robot, we took Raibert's three part control algorithm and applied some hardware specific modifications. Experimental results with the ARL Monopod demonstrate the effectiveness of these controllers.

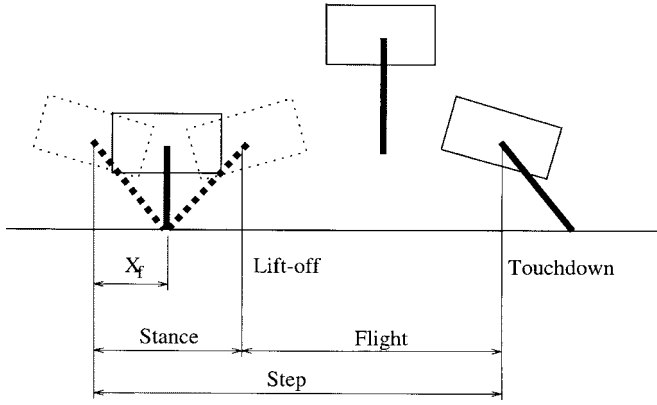


Fig. 3. Phases of Robot Running. The running motion of a legged system is comprised of a *stance phase* during which the leg is in contact with the ground and a ballistic *flight phase*. A *step* comprises one stance phase between *touchdown* and *lift-off* of the leg, and one flight phase beginning with *lift-off* and ending at the next *touchdown*.

### A. Hopping Height Control

The motors which actuate the leg spring and hip angle behave like ideal “torquers,” that is, we can control instantaneous current up to the thermal and operational limits imposed by the motor construction and the drive electronics. Since we operate intermittently we are able to draw the maximum stall torque of 1.8 Nm and utilize the operational regime for short term operation in the first quadrant given by the manufacturer and verified experimentally as

$$\tau \begin{cases} \leq \hat{\tau}(1 - \omega/\hat{\omega}) & \text{First quadrant} \\ \leq \hat{\tau} & \text{Second quadrant} \\ \geq -\hat{\tau}(1 + \omega/\hat{\omega}) & \text{Third quadrant} \\ \geq -\hat{\tau} & \text{Fourth quadrant.} \end{cases} \quad (2)$$

The same qualitative limits apply to other motors in this class of fractional horsepower motors. It is therefore evident that the traditional actuator limit of the form

$$\|\tau\| \leq \hat{\tau}$$

is not applicable to this class of electric dc motor which is increasingly common for driving small to medium size robots and mechanisms.

The controller in [5] calls for a fixed position step increment of the leg actuator at each maximum leg spring compression. The ensuing additional leg spring compression injects energy into the system. The vertical oscillation stabilizes around an operating point, where the losses during a complete cycle are balanced by the added energy. The stability of this approach has been investigated in [10]–[12].

Since the ground force against the leg actuator at maximum compression is approximately 500 N, a position step is an impractical strategy with low power electric actuators. Instead, we adopted a new open loop controller

$$\tau = \bar{\tau} \left(1 - \frac{\omega}{\hat{\omega}}\right)$$

which specifies a scaled version of the maximum torque-speed curve of our motor (2), with  $0 \leq \bar{\tau} < \hat{\tau}$  in the first quadrant (stance). This strategy is exactly implementable,

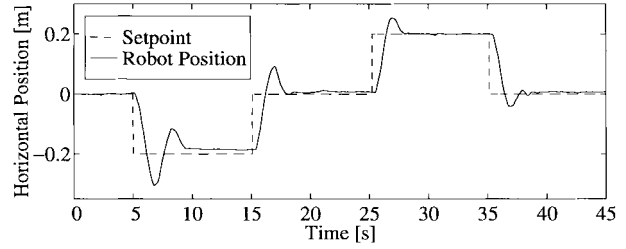


Fig. 4. Horizontal position regulation. The ARL Monopod tracks position steps equal to 1/3 the leg length.

applies thrust continuously during the entire stance phase and greatly reduces the required peak power. For our experiments we chose  $\bar{\tau} = 1$  Nm where  $\hat{\tau} = 1.8$  Nm.

### B. Speed Control

Forward speed is controlled by strategically servoing the toe touchdown position with respect to the hip  $x_f$  around the *neutral point*  $x_{fo} = \dot{x}T_s/2$ , where  $\dot{x}$  is the forward velocity and  $T_s$  is the previous stance time [5]. The resulting controller is

$$x_f = \frac{\dot{x}T_s}{2} + \kappa_{\dot{x}}(\dot{x} - \dot{x}_d)$$

where  $\kappa_{\dot{x}}$  is an empirically tuned gain and  $\dot{x}_d$  is the desired running speed. Since our robot runs on a treadmill, the actual and desired robot velocities,  $\dot{x}$ ,  $\dot{x}_d$  are replaced with the actual and desired robot velocities with respect to the treadmill,  $\dot{x}'$ ,  $\dot{x}'_d$ , and we add an integral position error term  $\kappa'_x(x' - x'_d)$ , to keep the robot near the center of the treadmill

$$x_f = \frac{\dot{x}'T_s}{2} + \kappa'_x(x' - x'_d) + \kappa'_{\dot{x}}(\dot{x}' - \dot{x}'_d). \quad (3)$$

The first planar experiments, shown in Fig. 4, were performed with zero treadmill speed. This data validates the successful overall system design, comprising the mechanical design of the body and hip actuation as well as the vertical hopping height controller. In addition, good position tracking performance is achieved via (3).

However, the true utility of this control law is for velocity tracking. Fig. 5 presents experimental data for robot running on the treadmill. Once the desired vertical hopping height is achieved, the treadmill speed is increased to 1 m/s and then reduced back to zero. The lower curve presents the robot position relative to the treadmill center. The robot stays within 0.15 m of the desired position—a small error compared to the total 26 m distance traversed.

### C. Pitch Control

The hip actuator is used during stance to regulate the pitching motion of the robot body. Raibert used a PD controller to compute the torque of the hip actuator,  $\tau$ , necessary to keep the robot body steady and horizontal

$$\tau = \kappa_p(\phi_d - \phi) - \kappa_d\dot{\phi}$$

where  $\phi_d$  is the desired hip angle,  $\phi$  and  $\dot{\phi}$  are the hip angle and rate, respectively, and  $\kappa_p$  is an empirically tuned gain. This

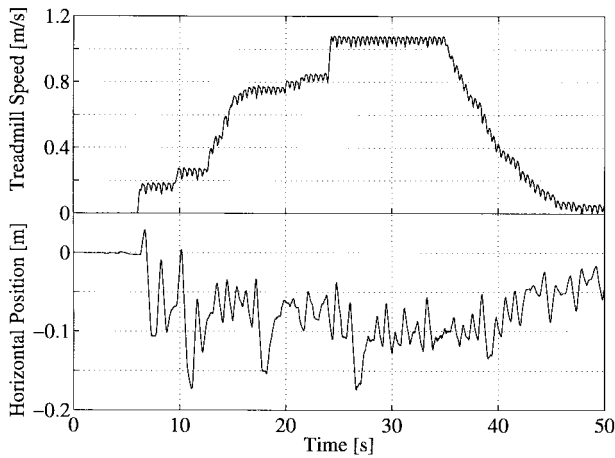


Fig. 5. Velocity tracking. The treadmill speed is manually adjusted from zero, vertical hopping, to 1 m/s and back to zero.

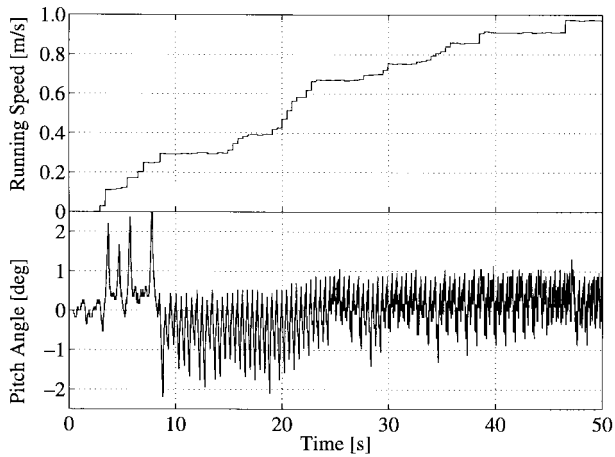


Fig. 6. Body pitching during robot running. The cyclic pitching motion of the robot body about the hip is kept to an amplitude of  $5^\circ$  while the robot speed increases to 1 m/s.

controller remained unchanged for our experiments shown in Fig. 6. The lower curve shows the cyclic oscillations of the robot body as the forward speed (upper curve) increases to 1 m/s. Despite the large variation in speed, the pitching oscillation of the robot body is kept within only  $\pm 2.5^\circ$  throughout the entire run. Control of body pitch during the stance phase is critical to stable running, since any nonzero pitch velocity will continue during flight and integrate to a potentially irrecoverable pitch error at the subsequent touchdown.

#### IV. POWER AND ENERGY

The use of low power electric motors for actuation distinguishes the ARL Monopod from most other dynamically stable legged machines which use hydraulics. This low-power approach to actuation motivates a detailed energetic study of the motion of our robot. How much energy is used for robot locomotion? How is this energy related to running speed? The answers to these questions should provide insights useful to further improving the energetic performance of the robot. Moreover, much of what is learned here about how this particular robot uses energy may be more generally applied

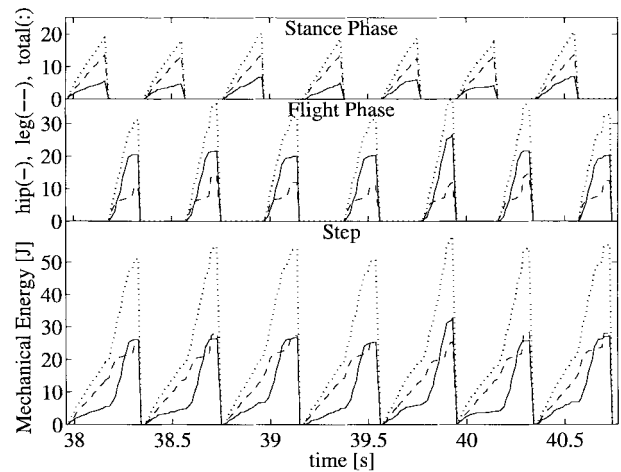


Fig. 7. Hip and leg energy at 1.2 m/s.

TABLE II  
ENERGY COST OF 50 J PER STEP DIVIDED BY PHASE AND ACTUATOR

	<i>Stance Phase</i>	<i>Flight Phase</i>
<i>Leg Motor</i>	Hopping Height: 13J	Leg Retraction: 12J
<i>Hip Motor</i>	Body Pitch: 5J	Forward Speed: 20J

in the mechanical design and controller development of future legged machines.

First, we will investigate the mechanical power and energy delivered to the system by the leg and hip motors. This “shaft power” is the mechanical output of the motor, the product of motor torque  $\tau$  and shaft speed  $\omega$

$$P = |\tau\omega| \quad (4)$$

and is related to the input electrical power via the combined motor-gear efficiency. Output power is a conventional measure of vehicle performance and can be easily computed from our available data. In addition, the results and insights are not dependent on any specific type of actuator.

We integrate (4) to calculate the energy added to the system by each of the motors as

$$E(t) = \int_{t_0}^t P(\sigma) d\sigma \quad (5)$$

where  $t_0 = t_{td}$  for the stance phase, and  $t_0 = t_{to}$  for the flight phase. The mean mechanical power delivered during a step can then be computed as

$$\bar{P}_{\text{step}} = \frac{E_{\text{step}}}{t_{\text{step}}} = \frac{E_{\text{stance}} + E_{\text{flight}}}{t_{\text{step}}} \quad (6)$$

Since the three control algorithms are decoupled (vertical motion and pitch control during stance, foot placement for velocity control during flight), the energetic cost of each control action is available for individual scrutiny. Such an analysis provides valuable insights into where energy is used most effectively and where energy can be saved. Equation (5) was applied to data obtained during a run with a top speed of 1.2 m/s to generate the energy output values plotted in Fig. 7 and summarized in Table II. The seven steps shown represent typical data for steady running.

The *leg motor* maintains the vertical motion during *stance* by compressing the leg spring. The energetic cost is given in the top field in Fig. 7 by the dashed curves, and amounts to a total of 13 J. During *flight*, the dashed curve in the middle field represents the energy involved in back-driving the leg actuator for the next stance phase. With 12 J, almost as much energy is used here to back-drive the actuator as to maintain the vertical motion! This is due to the large rotational energy stored in the combined inertia of the motor and ball screw at the end of the stance phase. Moreover, the peak power, indicated by the slope of the energy curve, is higher during flight,  $P_{\text{flight}} \approx 250$  W, compared to  $P_{\text{stance}} \approx 100$  W during stance. However, its nominal level is lower—less than 50 W—during most of the flight phase. Clearly, energy could be saved if a ballscrew with lower inertia could be used, and it would be back-driven slowly to exploit the compressed spring’s force for this purpose. The latter strategy would drastically reduce the peak power requirements.

The *hip motor* controls the body pitch during *stance*. The energetic cost is shown by the solid curve in the upper field of Fig. 7 and accounts for approximately 5 J at 1.2 m/s. During *flight*, the hip motor controls forward speed via the foot placement algorithm at the lion share of the energetic cost of 20 J! Since there is no compliance in series with the hip motor, it has to provide the entire energy for the leg swing motion. In the process its power output peaks at  $\approx 400$  W, then decreases in the flat region as touchdown approaches. Again, peak power requirements can be reduced considerably by commanding a smooth trajectory, as opposed to the set point from the foot placement algorithm. More importantly, the most drastic energy savings could come from adding a compliance in series with the hip actuator, such that during steady state operation, most of the 20 J expended by the hip actuator could be saved. Since this energetic cost increases with speed, so would the energy savings.

The mean mechanical power output of both motors was computed using (6) for 13 experimental runs—a total of 1306 steps. The resulting values of mean power are plotted against running speed in the upper field of Fig. 8 and form the basis for the specific resistance calculation below. Each point in the plot represents a single step while the solid line shows the least squares linear fit to the data. The dashed lines suggest upper and lower bounds for mean power output and enclose 98% of the data points. It is evident from the data that mean power increases with running speed. The reason for this is that the foot placement algorithm increases the leg angle setpoint with increasing running speed and therefore the overall amplitude of leg oscillation. At zero speed, only the hopping height controller is active and accounts for all the power shown in Fig. 8. The increase of mean power from  $\approx 58$  W at zero running speed to  $\bar{P}(1.2 \text{ m/s}) = 50 \text{ J}/0.4 \text{ s} \approx 125$  W is almost entirely due to the hip motor.

## V. SPECIFIC RESISTANCE

To evaluate the energetic performance of the ARL Monopod, it is interesting to compare it to other machines. A fair measure for comparison should include not only the

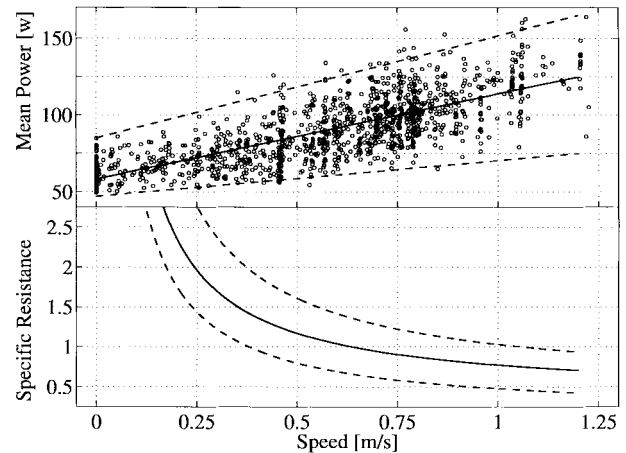


Fig. 8. Power output and specific resistance.

cost of locomotion in terms of output power but also the mass moved and the velocity attained. Such a measure, the *specific resistance*  $\varepsilon$ , was proposed in 1950 by Gabrielli and von Kármán [13]. It is defined as the ratio of power output,  $P$ , and the product of maximum speed,  $v_{\text{max}}$ , and vehicle weight  $m g$ ,  $\varepsilon = P/(m g v_{\text{max}})$  and can be used to compare vehicles regardless of size, speed or configuration. By plotting  $\varepsilon$  against speed Gabrielli and von Kármán compared the energetic performance of land, air and sea vehicles as well as biological systems on the same scale. We will be using the more general measure

$$\varepsilon(v) = \frac{P(v)}{m g v} \quad (7)$$

which allows us to scrutinize the energetics of the ARL Monopod over a whole range of velocities. We can now evaluate its energetic performance from the power output data in the upper field of Fig. 8. The resulting specific resistance is presented in the lower field as a function of running speed. Even though the mean power increases with speed,  $\varepsilon$  decreases steadily. The decrease of  $\varepsilon$  with speed suggests that the robot uses energy more efficiently the faster it runs. This trend can be understood by considering the power used to maintain the vertical motion. This power is an almost speed independent and constant “overhead cost.” It exists even at zero speed, where the specific resistance tends toward infinity. As the running speed increases, the power also increases but the change is small compared to the overall power output so that  $\varepsilon$  decreases. At 1.2 m/s the leg motor power accounts for half the overall energetic cost and the specific resistance reaches its lowest value of  $\varepsilon = 0.7$ . This value can be computed from (7) as

$$\varepsilon = \frac{125 \text{ W}}{15 \text{ kg } 9.81 \text{ m/s}^2 1.2 \text{ m/s}} \approx 0.7.$$

Values of  $\varepsilon$  at lower speeds may be reduced by specifying a lower hopping height, which was kept constant in these experiments to maintain a steady step duration.

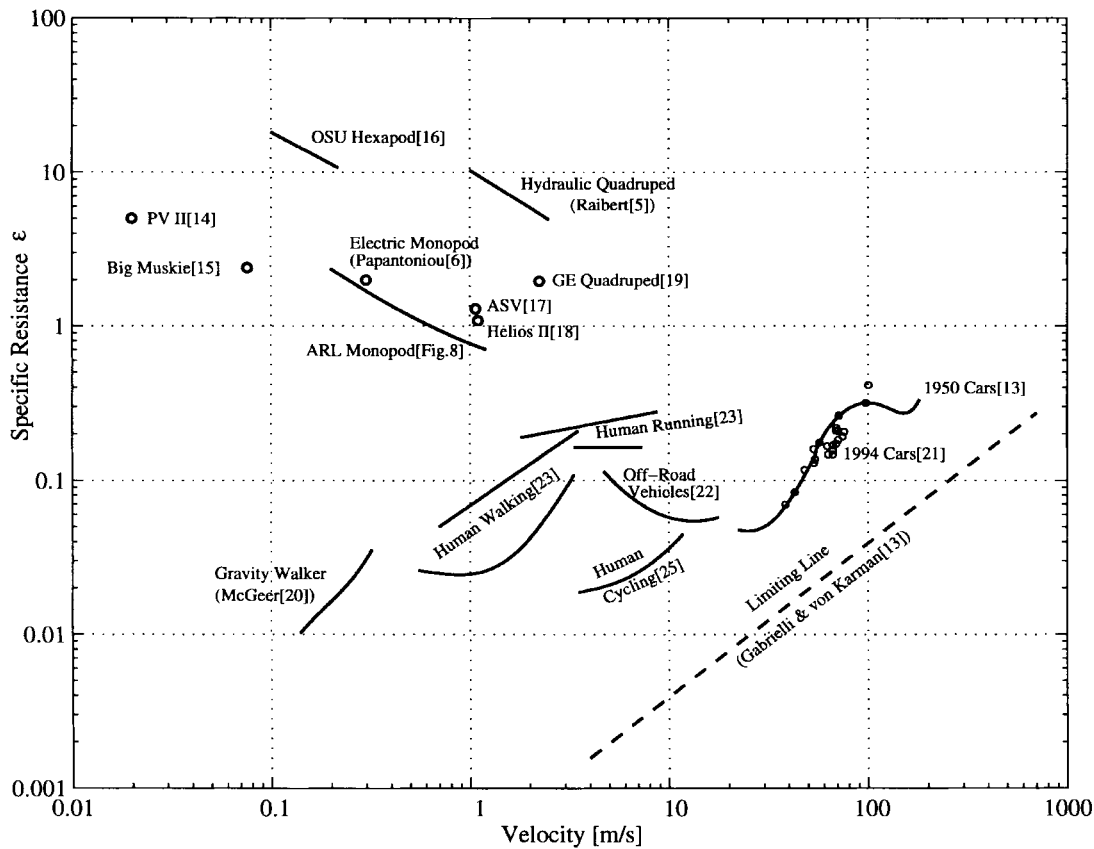


Fig. 9. Specific resistance for selected land vehicles.

In order to put the computed specific resistance in perspective, Fig. 9 shows selected land vehicles on a log-log scale. Some of today's legged machines (static walkers as well as dynamic walkers) appear prominently in the upper left hand corner far from the Gabrielli and von Kármán limiting line (GvK line)—a practical limit to vehicle performance based on 1950 data. Hirose's PV II [14] is a 10 kg quadruped with pantograph legs; Big Muskie [15] is a 12 200 000 kg coal mining dragline; The OSU Hexapod [16] is a 130 kg, six-legged static walker; Papantoniou [6] built a planar electrically actuated monopod which uses a gait termed "compliant walk" to move in the plane with a top speed of 0.3 m/s; The Active Suspension Vehicle (ASV) [17] was built at Ohio State University after the OSU hexapod. The six-legged ASV is a 2700 kg power autonomous static walker capable of moving over rough terrain and carrying a 230 kg pay load; Hirose's Helios II [18] has four independently articulated and controlled tracks; The 1350 kg hydraulic GE Quadraped [19] was built in 1968 and relied entirely on an operator to control each of its limbs via force reflective teleoperation; Raibert's hydraulic quadruped [5] weighs only 25 kg and is capable of *trotting*, *pacing*, and *bounding*; McGeer's "gravity walker" [20] appears as much as three orders of magnitude below the other legged machines. This unpowered 3.5 kg mechanism walks down an inclined plane driven entirely by gravity. Notwithstanding McGeer's unpowered device, our ARL Monopod with  $\varepsilon(1.2 \text{ m/s}) = 0.7$  currently has the

lowest specific resistance among the actively powered (and controlled) legged vehicles surveyed. For a more in-depth discussion and detailed description of the individual robots see [21].

Since legged machines are proposed as an alternative to conventional wheeled vehicles, their performance must be compared against these vehicles. The data includes "off-road vehicles" [22], "1950 Cars" [13] and "1994 Cars" from specifications published by selected auto manufacturers. The results range from  $\varepsilon = 0.4$  for a McLaren F1 down to  $\varepsilon = 0.07$  for a Volkswagen Eurovan Diesel. A complete table of source data for the individual cars is given in [21].

Although legged machines are studied as an alternative to wheeled systems, it is instructive to compare machine locomotion with human locomotion. The upper and lower curves for walking and running are from Cavagna [23] and Margaria [24], respectively. The data for human cycling is from Pugh [25]. It is noteworthy that the cycling data for  $\varepsilon$  relates more closely to that for cars than for humans. This suggests that the type of motion is more important than the power source in determining the specific resistance and implies that for each type of locomotion there is an optimal performance regardless of the type of prime mover.

It is important to realize that while we have taken every effort to accumulate the most accurate data possible for each vehicle, the results are still not clear cut. The difficulty arises from the inability of  $\varepsilon$  to account for the different methods

of computing output power for each type of vehicle. For cars, the quoted maximum power does not usually correspond to operation at maximum speed but rather at maximum acceleration. Some of the other vehicles have short term power storage devices such as a hydraulic accumulator or a flywheel which lower the mean power consumption while supplying peak power requirements. Moreover, conventional vehicles carry their power sources on board while most legged machines do not. There is a great advantage to not having to move the extra mass of a power source at top speed. Also, the additional mass of this power source is not included in the vehicle mass and is not revealed by the value of  $\epsilon$ . Many vehicles have parasitic power losses which do not contribute directly to locomotion but drain the available power and increase  $\epsilon$ . All these issues conspire to reduce the quantitative analysis portrayed in Fig. 9 to something more qualitative. In short, while the values of  $\epsilon$  have been computed from the best available data,  $\epsilon$  does not tell the entire energetic story; one should be wary of drawing sweeping conclusions from the data. Nevertheless, specific resistance remains a standard parameter for comparing energetic performance and is used by many authors to evaluate the performance of legged vehicles.

To summarize, it is clear that legged vehicles have a long way to go before they successfully compete with conventional off-road vehicles or biological systems on the basis of specific resistance.

## VI. CONCLUSION

Experiments with the ARL Monopod have shown that electric actuation for dynamically stable legged robots is feasible despite severe power limitations. This is possible by approaching the task as a system design problem, where the mechanical design and the controller design are closely coupled. This effort has resulted in the fastest electrically actuated legged robots with the best energetic performance, as measured by specific resistance, among all powered legged machines. Moreover, the energetic performance of the machine can be improved considerably, motivated by our experimental results and energetic analysis. For example, a promising strategy for minimizing energy cost involves implementing passive running with a hip compliance as proposed in [26] and continued in [9]. In this fashion, much of the hip swing motion, which consumes 40% of the total energy at our current top speed, can be provided by the natural oscillation of a spring-mass system. Our work suggests that a focussed effort toward energy minimization will lead to fully autonomous, electrically actuated, dynamically balanced legged robots in the near future.

## REFERENCES

- [1] R. B. McGhee and G. I. Iswandhi, "Adaptive locomotion of a multi-legged robot over rough terrain," *IEEE Trans. Syst., Man, Cybern.*, vol. SMC-9, pp. 176–182, Apr. 1979.
- [2] M. H. Kaplan and H. S. Seifert, "Hopping transporters for lunar exploration," *J. Spacecraft*, vol. 6, pp. 917–922, Aug 1969.
- [3] K. Matsuoka, "A mechanical model of repetitive hopping movements," *Biomechanisms*, vol. 5, pp. 251–258, 1980.

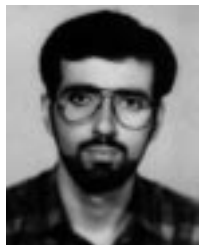
- [4] H. Miura and I. Shimoyama, "Dynamic walk of a biped," *Int. J. Robot. Res.*, vol. 3, no. 2, pp. 60–74, 1984.
- [5] M. H. Raibert, *Legged Robots That Balance*. Cambridge, MA: MIT Press, 1986.
- [6] K. V. Pappantoniou, "Electromechanical design for an electrically powered, actively balanced one leg planar robot," in *Proc. IEEE/RSJ Conf. Intelligent Systems Robots*, Osaka, Japan, 1991, pp. 1553–1560.
- [7] H. Rad, P. Gregorio, and M. Buehler, "Design, modeling and control of a hopping robot," in *Proc. IEEE/RSJ Conf. Intelligent Systems Robots*, Yokohama, Japan, July 1993, pp. 1778–1785.
- [8] M. Buehler, L. Whitcomb, F. Levin, and D. E. Koditschek, "A distributed message passing computational and I/O engine for real-time motion control," in *American Control Conf.*, Pittsburgh, PA, June 1989, pp. 478–483.
- [9] M. Ahmadi and M. Buehler, "A control strategy for stable passive running," in *Proc. IEEE Conf. Intelligent Systems Robots*, Pittsburgh, PA, Aug 1995, pp. 152–157.
- [10] D. E. Koditschek and M. Buehler, "Analysis of a simplified hopping robot," *Int. J. Robot. Res.*, vol. 10, pp. 587–605, Dec. 1991.
- [11] A. F. Vakakis and J. W. Burdick, "Chaotic motions of a simplified hopping robot," in *Proc. IEEE Int. Conf. Robotics Automation*, Cincinnati, OH, 1990, pp. 1464–1469.
- [12] V. V. Lashin, "Vertical and horizontal motion control of a one-legged hopping machine," *Int. J. Robot. Res.*, vol. 11, no. 5, pp. 491–498, 1992.
- [13] G. Gabrielli and T. H. von Karman, "What price speed?," *Mech. Eng.*, vol. 72, no. 10, pp. 775–781, 1950.
- [14] S. Hirose and Y. Umetani, "The basic motion regulation system for a quadruped walking machine," in *Design Engineering Tech. Conf. ASME*, Los Angeles, CA, 1980, paper 80-DET-34, pp. 1–6.
- [15] W. Cox, "Big muskie," *Ohio State Engineer*, pp. 25–52, Jan 1970.
- [16] K. J. Waldron *et al.*, "Configuration design of the adaptive suspension vehicle," *Int. J. Robot. Res.*, vol. 3, no. 2, pp. 37–48, 1984.
- [17] D. R. Pugh *et al.*, "Technical description of the adaptive suspension vehicle," *Int. J. Robot. Res.*, vol. 9, pp. 24–42, Apr. 1990.
- [18] S. Hirose, S. Aoki, and J. Miyake, "Terrain adaptive quadru-track vehicle Helios II," in *Int. Symp. Industrial Robots*, Tokyo, Japan, Oct. 1989, pp. 235–243.
- [19] R. S. Mosher, "Test and evaluation of a versatile walking truck," in *Proc. Off-Road Mobility Research Symp.*, Washington, DC, 1968, Int. Soc. Terrain Vehicle Systems, pp. 359–379.
- [20] T. McGeer, "Passive dynamic walking," *Int. J. Robot. Res.*, vol. 9, no. 2, pp. 62–82, 1990.
- [21] P. Gregorio, "Design, control and energy minimization strategies for an electrically actuated legged robot," M.Eng. thesis, McGill Univ., Montreal, P.Q., Canada, Aug. 1994.
- [22] M. G. Bekker, *Introduction to Terrain-Vehicle Systems*. Ann Arbor, MI: Univ. of Michigan Press, 1969.
- [23] G. A. Cavagna and M. Kaneko, "Mechanical work and efficiency in level walking and running," *J. Physiol.*, vol. 268, pp. 467–481, 1977.
- [24] R. Margaria, *Biomechanics and Energetics of Muscular Exercise*. Oxford, U.K.: Oxford Univ. Press, 1976.
- [25] L. Pugh, "The relation of oxygen intake and speed in competition cycling and comparative observations on the bicycle ergometer," *J. Physiol.*, vol. 241, pp. 795–808, 1974.
- [26] M. H. Raibert and C. M. Thompson, "Passive dynamic running," in *Experimental Robotics I*, V. Hayward and O. Khatib, Eds. New York: Springer-Verlag, 1989, pp. 74–83.



space shuttle mission.

**Pedro Gregorio** received the B.Eng and M.Eng. degrees in mechanical engineering in 1992 and 1995, respectively, from McGill University, Montreal, P.Q., Canada.

He is with Solutions by Design, Montreal, a consulting firm which offers mechanical design services. Recent projects completed for the Canadian Space Agency include three DOF force reflecting hand controllers, a free-floating robot to simulate space operations, and support hardware for the CFZF, an experimental payload aboard the STS-77



**Mojtaba Ahmadi** was born in Tehran, Iran, in 1965. He received the B.S. degree from Sharif University of Technology, Tehran, in 1988 and the M.S. degree from the University of Tehran in 1992, both in mechanical engineering. He is currently pursuing the Ph.D. degree at McGill University, Montreal, P.Q., Canada.

He has worked on the simulation of mechanical systems at the Industrial Research Institute, Tehran, and has been a Technical Consultant with the Ports and Shipping Organization, Iran. He is now a Research Assistant in the Ambulatory Robotics Lab in the Center for Intelligent Machines, McGill University. He is currently working on stable control of legged systems with joint compliance.



**Martin Buehler** (S'85–M'90) was born in Lahr, Germany, in 1961. He received the M.Sc. and Ph.D. degrees in electrical engineering from Yale University, New Haven, CT, in 1985 and 1990, respectively.

Until 1991, he was a Postdoctoral Associate in the LegLab in the Artificial Intelligence Lab, Massachusetts Institute of Technology, Cambridge. Since 1991, he has been an Assistant Professor with the Department of Mechanical Engineering, McGill University, Montreal, P.Q., Canada. His research

interests are in the areas of robot manipulation and legged locomotion.

Dr. Buehler held a Junior Industrial Research Chair from 1991 to 1995 and is a Scholar of the Canadian Institute for Advanced Research. He is currently the Project Leader for Machine Sensing I, an IRIS/PRECARN project of the Federal Network of Centres of Excellence.